

# Generalized Task-Parameterized Movement Primitives

Yanlong Huang, João Silvério, Leonel Rozo, and Darwin G. Caldwell

**Abstract** Programming by demonstrations has recently gained much attention due to its user-friendly and natural way to transfer human skills to robots. In order to facilitate the learning of multiple demonstrations and meanwhile generalize to new situations, a task-parameterized movement learning has been recently developed [4], which has achieved reliable performance in areas such as human-robot collaboration and robot bimanual operation. However, the crucial task frames and associated task parameters in this learning framework are often set based on human experience, which renders three problems that have not been addressed yet: *(i)* task frames are treated equally without considering the task priorities; *(ii)* task parameters are defined without considering additional task constraints, e.g., robot joint limits and motion smoothness; *(iii)* a fixed number of task frames are pre-defined regardless some of them are redundant or even irrelevant for the task at hand. In this paper, we generalize the task-parameterized learning by addressing the aforementioned problems. Moreover, we provide an alternative way to refine and adapt previously learned robot skills, which allows us to work on a low dimensional space. Several examples are studied in simulated and real robotic systems, showing the applicability of our approach.

## 1 Introduction

As an intuitive and user-friendly way to endow a robot with skills from humans, Programming by Demonstration (PbD) has become appealing in the past few years [1]. The basic idea of PbD is to extract the important or consistent features from demonstrations and then adapt them to various situations, which is also referred to as generalization. In practice, a myriad of robot tasks are formulated as a regression problem, e.g., a mapping from sensory information to robot (motor) actions. How-

---

All authors are with Department of Advanced Robotics, Istituto Italiano di Tecnologia, Via Morego 30, 16163 Genoa, Italy, e-mail: firstname.lastname@iit.it

ever, typical regression approaches (e.g. locally weighted regression (LWR) [2] or Gaussian process regression (GPR) [11]) may suffer from limited extrapolation capabilities [4]. In order to adapt human demonstrations to a broader range of task instances, a multi-frame based probabilistic movement learning framework, formally called task-parameterized Gaussian mixture model (TP-GMM), has been proposed [4]. This approach exploits local consistent features among demonstrations in different task-frames (which might be interpreted as local frames) instead of using a single global reference frame, and subsequently transfers local features to new task frames (which in turn describe new task situations), yielding reliable performance for both interpolation and extrapolation.

However, within the learning framework of TP-GMM [4], the crucial task frames and associated parameters are usually set based on human knowledge about the task, which renders three main limitations: (i) task frames are treated equally without considering the task priorities. Note that, depending on human interpretation of tasks, the task frames influence may vary over time, which can be interpreted as the expertise or *confidence* that a specific frame has with respect to a portion of the task; (ii) task parameters are defined without considering additional task constraints, e.g., robot joint limits and motion smoothness. These new constraints demand the robot to adapt the learned task-parameterized skill according to the additional requirements while performing the task successfully; (iii) a fixed number of task frames are pre-defined regardless some of them are redundant or even irrelevant for the task at hand. These undesired frames will increase the computational burden and probably degrade the overall performance of TP-GMM.

Beside the foregoing problems, it is worth mentioning that human demonstrations might not be optimal for the robot. Namely, the demonstrator may mainly focus on the task at hand while the robot capability is not fully exploited, which may lead to high energy movements, unnecessary large joint displacements, or high torque motion, among other problems. However, due to the complicated structure or non-linearity exhibited in the demonstrated trajectories, it is non-trivial to optimize these trajectories effectively. We here propose to take advantage of the task-parametrized formulation of TP-GMM by optimizing task parameters instead of directly modifying the model parameters (i.e., GMM means and covariance matrices), while the latter is conventionally done [6]. A clear advantage of our approach is that task parameters lie in a lower dimensional space compared to that of trajectory model parameters.

In this paper, we first briefly introduce TP-GMM (Section 2). Subsequently, we re-formulate TP-GMM as task-parametrized local trajectories (Section 3.1) so as to address the stated problems properly. Using the new framework, we propose a confidence-weighted scheme to address the problem (i) (Section 3.2). In order to cope with problem (ii), we formulate the optimization of task parameters as a reinforcement learning (RL) problem (Section 4.1), with the aim of enabling the robot to finish the task while satisfying additional task constraints. Also, we provide a dual perspective to show that the optimization of task parameters in a lower dimensional space is equivalent to that of model parameters in a higher dimensional space (Section 4.2). Furthermore, as a solution to problem (iii) we propose an iterative frame

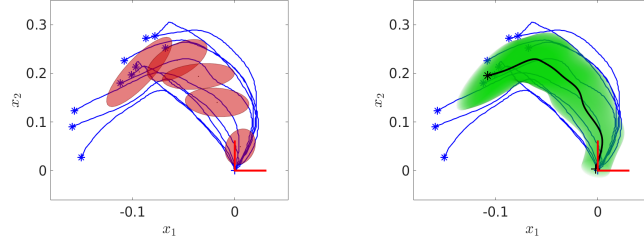


**Fig. 1** Illustrations of trajectory encoding using GMM (*left* plot) and trajectory retrieval using GMR (*right* plot). The blue curves represent human demonstrations, ‘\*’ and ‘+’ denote the start and end points of trajectories, respectively. The ellipses in the *left* graph depict GMM components and the black solid curve in the *right* figure represents the mean trajectory retrieved by GMR.

selection algorithm to exploit the most task-relevant frames (Section 5), where the task frame optimization is used. Finally, we evaluate our approaches through several examples in Section 6 and conclude this paper in Section 7.

## 2 An Overview of Task-parameterized Gaussian Mixture Model

In the context of imitation learning, one crucial ingredient is the consistent features underlying human demonstrations [4, 6, 7]. In order to facilitate the extraction of consistent features, TP-GMM has been exploited in numerous works, e.g., the human-robot collaborative transportation [9] as well as the robot bimanual sweeping task [12]. Often, a set of candidate task frames (e.g., frames at target objects [9] or robot end-effectors [12]) needs to be pre-defined for the implementation of TP-GMM.

Formally, let us consider  $P$  task frames, and refer to the rotation matrix  $\mathbf{A}_t^{(j)}$  and translation vector  $\mathbf{b}_t^{(j)}$  of each frame  $\{j\}$  with respect to the global reference frame  $\{O\}$  as the *task parameters*, where  $t$  denotes the time step and  $j = 1, 2, \dots, P$ . We can project human demonstrations  $\{\{\xi_{t,m}\}_{t=1}^N\}_{m=1}^M$  into each frame separately and subsequently exploit the local features in different frames. Here,  $N$  and  $M$  respectively represent the time length of each demonstration and the number of demonstrations, while  $\xi_{t,m} \in \mathbb{R}^D$  represents a  $D$ -dimensional trajectory point. The projected trajectories in each frame  $\{j\}$  are computed by [4]

$$\xi_{t,m}^{(j)} = (\mathbf{A}_t^{(j)})^{-1}(\xi_{t,m} - \mathbf{b}_t^{(j)}). \quad (1)$$

If we consider the estimation of consistent features among the projected trajectories from a probabilistic perspective, GMM can be employed [4, 8, 9, 12], which has shown reliable modeling of joint distribution of trajectories. By using *expectation maximization* (EM) algorithm, GMM parameters  $\{\pi_k, \{\mu_k^{(j)}, \Sigma_k^{(j)}\}_{j=1}^P\}_{k=1}^K$  in different frames can be estimated, where  $K$  represents the number of Gaussian

components,  $\pi_k$ ,  $\boldsymbol{\mu}_k^{(j)}$  and  $\boldsymbol{\Sigma}_k^{(j)}$  respectively denote mixture coefficients, Gaussian centers and covariance matrices in each frame  $\{j\}$ .

By using affine transformations and product of Gaussian, the new GMM components  $\{\pi_k, \boldsymbol{\mu}_{k,t}, \boldsymbol{\Sigma}_{k,t}\}_{k=1}^K$  at time  $t$  in the global frame  $\{O\}$  can be computed as [4]

$$\mathcal{N}(\boldsymbol{\mu}_{k,t}, \boldsymbol{\Sigma}_{k,t}) \propto \prod_{j=1}^P \mathcal{N}(\mathbf{A}_t^{(j)} \boldsymbol{\mu}_k^{(j)} + \mathbf{b}_t^{(j)}, \mathbf{A}_t^{(j)} \boldsymbol{\Sigma}_k^{(j)} (\mathbf{A}_t^{(j)})^T), \quad (2)$$

which yields a distribution  $\boldsymbol{\xi}_t \sim \sum_{k=1}^K \pi_k \mathcal{N}(\boldsymbol{\mu}_{k,t}, \boldsymbol{\Sigma}_{k,t})$  in the frame  $\{O\}$ . Furthermore, we can decompose  $\boldsymbol{\xi}$  as the input  $\boldsymbol{\xi}_{\mathcal{I}}$  and the output  $\boldsymbol{\xi}_{\mathcal{O}}$ , and subsequently, we generate a trajectory in the global frame  $\{O\}$  as  $\boldsymbol{\xi}_{t,\mathcal{O}} | \boldsymbol{\xi}_{t,\mathcal{I}} \sim \mathcal{N}(\boldsymbol{\mu}_{t,\mathcal{O}}, \boldsymbol{\Sigma}_{t,\mathcal{O}})$  by using Gaussian mixture regression (GMR) [4, 5]. To name an example, if we consider  $\boldsymbol{\xi}_{\mathcal{I}}$  and  $\boldsymbol{\xi}_{\mathcal{O}}$  as time and a 3-D trajectory point, respectively, a sequence of trajectory points in frame  $\{O\}$  at different time steps can be generated. An illustration of trajectory encoding via GMM and trajectory retrieval via GMR in the  $x$ - $y$  plane is provided in Fig. 1. It can be observed from Fig. 1 (*left graph*) that, the fifth Gaussian component (counting from left to right) has the smallest covariance, implying that trajectory segments encapsulated by this component are highly consistent across demonstrations, and therefore represent an important feature of the movements. Note that the input is not limited to be time, other inputs can be possible depending on the task characteristics.

### 3 Task-parameterized Movement Primitives

In order to formulate the confidence assignments to task frames, optimization of task parameters as well as frame selection, we first introduce a novel re-formulation built on TP-GMM (Section 3.1), which we will refer to as the *task-parameterized movement primitives* (TMP). Subsequently, we propose the *confidence-weighted task-parameterized movement primitives* (CW-TMP) (Section 3.2) so as to assign task frames with different confidences.

#### 3.1 Task-parameterized Movement Primitives

Assuming that we can access to the local GMM models in different task frames, the local trajectory distribution in each frame  $\{j\}$  can be represented as  $\boldsymbol{\xi}^{(j)} \sim \sum_{k=1}^K \pi_k \mathcal{N}(\boldsymbol{\mu}_k^{(j)}, \boldsymbol{\Sigma}_k^{(j)})$ . By decomposing  $\boldsymbol{\xi}^{(j)}$  as the input  $\boldsymbol{\xi}_{\mathcal{I}}^{(j)}$  and the output  $\boldsymbol{\xi}_{\mathcal{O}}^{(j)}$ , we can generate a local trajectory in frame  $\{j\}$  as  $\boldsymbol{\xi}_{t,\mathcal{O}}^{(j)} | \boldsymbol{\xi}_{t,\mathcal{I}}^{(j)} \sim \mathcal{N}(\boldsymbol{\mu}_{t,\mathcal{O}}^{(j)}, \boldsymbol{\Sigma}_{t,\mathcal{O}}^{(j)})$  by using GMR. Inspired by the two-frame illustration of task-parameterized learning [4], we view the global trajectory as a trade-off among the local trajectories from different task frames. Formally, TMP estimates  $\boldsymbol{\xi}_{t,\mathcal{O}}$  by maximizing

$\prod_{j=1}^P \mathcal{P} \left( \xi_{t,\mathcal{O}} | \mathbf{A}_{t,\mathcal{O}}^{(j)} \mu_{t,\mathcal{O}}^{(j)} + \mathbf{b}_{t,\mathcal{O}}^{(j)}, \mathbf{A}_{t,\mathcal{O}}^{(j)} \Sigma_{t,\mathcal{O}}^{(j)} (\mathbf{A}_{t,\mathcal{O}}^{(j)})^T \right)$ . Through the logarithmic transformation, this objective can be solved by minimizing

$$\sum_{j=1}^P (\xi_{t,\mathcal{O}} - \mathbf{A}_{t,\mathcal{O}}^{(j)} \mu_{t,\mathcal{O}}^{(j)} - \mathbf{b}_{t,\mathcal{O}}^{(j)})^T (\mathbf{A}_{t,\mathcal{O}}^{(j)} \Sigma_{t,\mathcal{O}}^{(j)} (\mathbf{A}_{t,\mathcal{O}}^{(j)})^T)^{-1} (\xi_{t,\mathcal{O}} - \mathbf{A}_{t,\mathcal{O}}^{(j)} \mu_{t,\mathcal{O}}^{(j)} - \mathbf{b}_{t,\mathcal{O}}^{(j)}). \quad (3)$$

By calculating derivatives of (3) with respect to  $\xi_{t,\mathcal{O}}$ , the optimal solution can be derived, which is equivalent to the product of Gaussians, i.e.,

$$\xi_{t,\mathcal{O}} \sim \prod_{j=1}^P \mathcal{N} \left( \mathbf{A}_{t,\mathcal{O}}^{(j)} \mu_{t,\mathcal{O}}^{(j)} + \mathbf{b}_{t,\mathcal{O}}^{(j)}, \mathbf{A}_{t,\mathcal{O}}^{(j)} \Sigma_{t,\mathcal{O}}^{(j)} (\mathbf{A}_{t,\mathcal{O}}^{(j)})^T \right), \quad (4)$$

where  $\mathbf{A}_{t,\mathcal{O}}^{(j)}$  and  $\mathbf{b}_{t,\mathcal{O}}^{(j)}$  respectively correspond to the output blocks of  $\mathbf{A}_t^{(j)} = [(\mathbf{A}_{t,\mathcal{I}}^{(j)})^T (\mathbf{A}_{t,\mathcal{O}}^{(j)})^T]^T$  and  $\mathbf{b}_t^{(j)} = [(\mathbf{b}_{t,\mathcal{I}}^{(j)})^T (\mathbf{b}_{t,\mathcal{O}}^{(j)})^T]^T$ . Note that the input blocks  $\mathbf{A}_{t,\mathcal{I}}^{(j)}$  and  $\mathbf{b}_{t,\mathcal{I}}^{(j)}$  are used to retrieve the local desired inputs  $\xi_{t,\mathcal{I}}^{(j)}$  projected into the different task frames, which act as the conditional inputs for the generation of local trajectories. Let us emphasize that TMP is a trajectory-based approach where local trajectories encapsulate the consistency of the task in local frames, while TP-GMM [4] is exclusively built on local models. Moreover, TMP can be applied to other approaches that retrieve a Gaussian distribution of trajectories in local frames.

### 3.2 Confidence-weighted Task-parameterized Movement Primitives

Among previous works on the task-parameterized learning [4, 9, 12], task frames and associated parameters  $\{\mathbf{A}_t^{(j)}, \mathbf{b}_t^{(j)}\}$  are defined beforehand. Moreover, task frames are assigned with the same priorities. However, it may happen that, for some specific task frames, their influences are expected to be larger than the rest of frames, and hence it is desired to introduce human confidence for task frames. On the basis of TMP, the human prior information can be naturally incorporated into task frames, yielding CW-TMP. Assuming that the confidences of different task frames are known, let us denote them as  $\gamma_{t,j}$ , where  $\gamma_{t,j} \in (0, 1)$ . In contrast to the multinomial distribution and its application in trajectory mixture [10], we formulate the original objective of TMP as  $\prod_{j=1}^P \mathcal{P} \left( \xi_{t,\mathcal{O}} | \mathbf{A}_{t,\mathcal{O}}^{(j)} \mu_{t,\mathcal{O}}^{(j)} + \mathbf{b}_{t,\mathcal{O}}^{(j)}, \mathbf{A}_{t,\mathcal{O}}^{(j)} \Sigma_{t,\mathcal{O}}^{(j)} (\mathbf{A}_{t,\mathcal{O}}^{(j)})^T \right)^{\gamma_{t,j}}$ . Here,  $\gamma_{t,j}$  can be interpreted as a measurement of the contribution of each local conditional Gaussian distribution to the product operation. Similar to the derivation of (4), the optimal solution of CW-TMP can be determined by

$$\xi_{t,\mathcal{O}} \sim \prod_{j=1}^P \mathcal{N} \left( \mathbf{A}_{t,\mathcal{O}}^{(j)} \mu_{t,\mathcal{O}}^{(j)} + \mathbf{b}_{t,\mathcal{O}}^{(j)}, \mathbf{A}_{t,\mathcal{O}}^{(j)} (\Sigma_{t,\mathcal{O}}^{(j)} / \gamma_{t,j}) (\mathbf{A}_{t,\mathcal{O}}^{(j)})^T \right). \quad (5)$$

The above result has an intuitive interpretation: if the frame  $\{j\}$  has a higher (lower) confidence  $\gamma_{t,j}$  at time  $t$ , its contribution to the Gaussian product is higher (lower) due to a smaller (larger) covariance (i.e.,  $(\Sigma_{t,O}^{(j)}/\gamma_{t,j})$ ).

## 4 Optimization of Task-parameterized Movement Primitives

In this section we address the question: how can good task parameters be selected? For instance, for applications with flexible task parameters, i.e., different values of task parameters allow for finishing the same task, which values of parameters are better? We tackle this problem by optimizing task parameters from a reinforcement learning perspective (Section 4.1), and subsequently, we provide a dual perspective on this optimization, so that a connection between our approach and the standard optimization of GMM components is built (Section 4.2).

### 4.1 Reinforcement Learning of Task Parameters

Considering that task parameters  $\{\mathbf{A}_t^{(j)}, \mathbf{b}_t^{(j)}\}$  describe different task frames (and subsequently, different task situations), a straightforward way to refine them is by applying rotation and translation operations to their pre-defined values. Since the input blocks in task parameters are often uncontrollable (e.g., a time sequence input), we only discuss the learning of output blocks, i.e.,  $\{\mathbf{A}_{t,O}^{(j)}, \mathbf{b}_{t,O}^{(j)}\}$ . Formally, let us denote new rotation matrices and translational vectors as  $\{\mathbf{R}_t^{(j)}\}_{j=1}^P$  and  $\{\mathbf{d}_t^{(j)}\}_{j=1}^P$ . Then, for an arbitrary local trajectory point  $\xi_{t,O}^{(j)}$  in the frame  $\{j\}$ , after the new rotational and translational operations are performed, we can prove that its representation in the reference frame  $\{O\}$  becomes

$$\hat{\xi}_{t,O}^{(j)} = \underbrace{\mathbf{A}_{t,O}^{(j)} \mathbf{R}_t^{(j)}}_{\hat{\mathbf{A}}_{t,O}^{(j)}} \xi_{t,O}^{(j)} + \underbrace{\mathbf{A}_{t,O}^{(j)} \mathbf{d}_t^{(j)} + \mathbf{b}_{t,O}^{(j)}}_{\hat{\mathbf{b}}_{t,O}^{(j)}}. \quad (6)$$

Accordingly, new task parameters  $\{\hat{\mathbf{A}}_{t,O}^{(j)}, \hat{\mathbf{b}}_{t,O}^{(j)}\}$  of the frame  $\{j\}$  are determined, which can be later used to replace initial task parameters  $\{\mathbf{A}_{t,O}^{(j)}, \mathbf{b}_{t,O}^{(j)}\}$  and generate a new trajectory sequence in the frame  $\{O\}$  via (4). With the affine transformation in (6), we actually learn task parameters through finding the optimal rotation matrices  $\mathbf{R}_t^{(j)}$  and translational vectors  $\mathbf{d}_t^{(j)}$ .

We here consider that the rotation matrix represents sequential rotations along  $x, y$  and  $z$  axes with angles  $\alpha, \beta$  and  $\gamma$ , and therefore the determination of  $\{\mathbf{R}_t^{(j)}\}_{j=1}^P$  is equivalent to that of  $\{\alpha_t^{(j)}, \beta_t^{(j)}, \gamma_t^{(j)}\}_{j=1}^P$ . Furthermore, let us denote  $\mathbf{a}_t^{(j)} = [\alpha_t^{(j)} \ \beta_t^{(j)} \ \gamma_t^{(j)} \ \mathbf{d}_t^{(j)T}]$  and  $\mathbf{a}_t = [\mathbf{a}_t^{(1)} \ \mathbf{a}_t^{(2)} \ \dots \ \mathbf{a}_t^{(P)}]^T$ . In order to formulate the

learning of  $\mathbf{a}_t$  into a RL problem, we represent  $\mathbf{a}_t$  as a parametric policy, i.e.,

$$\mathbf{a}_t = \Phi_t(\boldsymbol{\theta} + \epsilon), \quad (7)$$

where  $\Phi_t$  and  $\epsilon$  represent basis functions and stochastic exploration noise, respectively, and  $\boldsymbol{\theta}$  denotes the policy parameters which needs to be learned. By optimizing the policy parameters  $\boldsymbol{\theta}$  with respect to additional constraints (i.e., task-dependent cost functions), the optimal parameters  $\mathbf{a}_t$  can be found, which are subsequently used to retrieve new task parameters based on (6).

For the typical policy search problem (7), many algorithms have been proven effective. Here, we take policy improvement with path integrals (PI<sup>2</sup>) [3, 14] as an example to illustrate the learning of task parameters. Let us denote the exploration noise at time step  $i \in \{1, 2, \dots, N\}$  during the roll-out (i.e., episode)  $h \in \{1, 2, \dots, H\}$  as  $\epsilon_{i,h}$ , where  $N$  is the time length of a roll-out and  $H$  is the number of roll-outs. As suggested in [13], we apply a constant exploration noise  $\epsilon_h$  during the  $h$ -th roll-out (i.e.,  $\epsilon_h = \epsilon_{i,h}, i \in \{1, 2, \dots, N\}$ ) and update the policy parameters using every  $H$  roll-outs. In each roll-out, we can first calculate  $\mathbf{a}_t$  using (7). Subsequently, we can retrieve new task parameters  $\{\hat{\mathbf{A}}_{t,\mathcal{O}}^{(j)}, \hat{\mathbf{b}}_{t,\mathcal{O}}^{(j)}\}_{j=1}^P$  using (6). By plugging new task parameters and local trajectories in different frames into (4), an updated trajectory in the reference frame can be generated. Moreover, on the basis of the cost function (which is usually pre-defined depending on the specific task and additional constraints), we can compute the cumulative cost value  $S_h$  for each roll-out. Given the cumulative costs  $\{S_h\}_{h=1}^H$  in  $H$  roll-outs, the policy parameters are updated by

$$\boldsymbol{\theta} := \boldsymbol{\theta} + \sum_{h=1}^H w_h \epsilon_h \quad (8)$$

with  $w_h = \frac{e^{-\kappa S_h}}{\sum_{h=1}^H e^{-\kappa S_h}}$ , where  $\kappa > 0$ . We can continuously do explorations and update  $\boldsymbol{\theta}$  every  $H$  roll-outs until  $\boldsymbol{\theta}$  converges or the cumulative cost is below a certain value. The complete learning procedure is illustrated in *Algorithm 1*.

## 4.2 Dual Perspective of Optimizing Task Parameters

In this section, we provide a dual perspective to interpret the optimization of task parameters. Before that, let us first recall the main result (2) in TP-GMM. It is noted that in (2), there exists an affine transformation of the GMM component  $\{\boldsymbol{\mu}_k^{(j)}, \boldsymbol{\Sigma}_k^{(j)}\}$  through the task parameters  $\{\mathbf{A}_t^{(j)}, \mathbf{b}_t^{(j)}\}$ . If we write  $\boldsymbol{\mu}_k^{(j)} = \begin{bmatrix} \boldsymbol{\mu}_{k,\mathcal{I}}^{(j)} \\ \boldsymbol{\mu}_{k,\mathcal{O}}^{(j)} \end{bmatrix}$ ,  $\boldsymbol{\Sigma}_k^{(j)} = \begin{bmatrix} \boldsymbol{\Sigma}_{k,\mathcal{I}\mathcal{I}}^{(j)} & \boldsymbol{\Sigma}_{k,\mathcal{I}\mathcal{O}}^{(j)} \\ \boldsymbol{\Sigma}_{k,\mathcal{O}\mathcal{I}}^{(j)} & \boldsymbol{\Sigma}_{k,\mathcal{O}\mathcal{O}}^{(j)} \end{bmatrix}$  and substitute the optimized task parameters  $\{\hat{\mathbf{A}}_{t,\mathcal{O}}^{(j)}, \hat{\mathbf{b}}_{t,\mathcal{O}}^{(j)}\}$  into (2), new mean and covariance can be derived as

**Algorithm 1** Optimization of task-parameterized movement primitives*Initialization*

- 1: Define a reference frame  $\{O\}$  and initial candidate task frames  $\{j\}_{j=1}^P$ .
- 2: Collect human demonstrations  $\{\{\xi_{t,m}\}_{t=1}^N\}_{m=1}^M$ .

*Phase 1: learn from demonstrations*

- 1: Project demonstrations into each frame via (1) separately.
- 2: Fit GMM to projected trajectories in each frame using EM and generate local trajectories (represented by conditional probabilities  $\mathcal{P}(\xi_{t,O}^{(j)}|\xi_{t,I}^{(j)})$ ) in different frames using GMR.

*Phase 2: generalization with optimized task parameters*

- 1: Determine new task parameters  $\{\{\mathbf{A}_t^{(j)}, \mathbf{b}_t^{(j)}\}_{t=1}^N\}_{j=1}^P$  depending on the new task at hand.
- 2: Optimize new task parameters using (8) so as to minimize the cost function (which is defined based on task requirements and additional constraints).
- 3: Use optimized task parameters  $\{\{\hat{\mathbf{A}}_{t,O}^{(j)}, \hat{\mathbf{b}}_{t,O}^{(j)}\}_{t=1}^N\}_{j=1}^P$ , combined with local trajectories in different task frames, to estimate  $\xi_{t,O}$  in  $\{O\}$  via (4).

$$\begin{aligned}\hat{\boldsymbol{\mu}}_{t,k}^{(j)} &= \begin{bmatrix} \mathbf{A}_{t,I}^{(j)} & \mathbf{0} \\ \mathbf{0} & \hat{\mathbf{A}}_{t,O}^{(j)} \end{bmatrix} \begin{bmatrix} \boldsymbol{\mu}_{k,I}^{(j)} \\ \boldsymbol{\mu}_{k,O}^{(j)} \end{bmatrix} + \begin{bmatrix} \mathbf{b}_{t,I}^{(j)} \\ \hat{\mathbf{b}}_{t,O}^{(j)} \end{bmatrix} \\ \hat{\boldsymbol{\Sigma}}_{t,k}^{(j)} &= \begin{bmatrix} \mathbf{A}_{t,I}^{(j)} & \mathbf{0} \\ \mathbf{0} & \hat{\mathbf{A}}_{t,O}^{(j)} \end{bmatrix} \begin{bmatrix} \boldsymbol{\Sigma}_{k,II}^{(j)} & \boldsymbol{\Sigma}_{k,IO}^{(j)} \\ \boldsymbol{\Sigma}_{k,OI}^{(j)} & \boldsymbol{\Sigma}_{k,OO}^{(j)} \end{bmatrix} \begin{bmatrix} \mathbf{A}_{t,I}^{(j)} & \mathbf{0} \\ \mathbf{0} & \hat{\mathbf{A}}_{t,O}^{(j)} \end{bmatrix}^T\end{aligned}\quad (9)$$

This new mean and covariance can also be seen as being equivalent to a new local model  $\{\hat{\boldsymbol{\mu}}_k^{(j)}, \hat{\boldsymbol{\Sigma}}_k^{(j)}\}$ , rotated and translated by the old parameters  $\{\mathbf{A}_t^{(j)}, \mathbf{b}_t^{(j)}\}$ , resulting in the equalities

$$\begin{aligned}\hat{\boldsymbol{\mu}}_{t,k}^{(j)} &= \begin{bmatrix} \mathbf{A}_{t,I}^{(j)} & \mathbf{0} \\ \mathbf{0} & \hat{\mathbf{A}}_{t,O}^{(j)} \end{bmatrix} \begin{bmatrix} \hat{\boldsymbol{\mu}}_{k,I}^{(j)} \\ \hat{\boldsymbol{\mu}}_{k,O}^{(j)} \end{bmatrix} + \begin{bmatrix} \mathbf{b}_{t,I}^{(j)} \\ \hat{\mathbf{b}}_{t,O}^{(j)} \end{bmatrix} \\ \hat{\boldsymbol{\Sigma}}_{t,k}^{(j)} &= \begin{bmatrix} \mathbf{A}_{t,I}^{(j)} & \mathbf{0} \\ \mathbf{0} & \hat{\mathbf{A}}_{t,O}^{(j)} \end{bmatrix} \begin{bmatrix} \hat{\boldsymbol{\Sigma}}_{k,II}^{(j)} & \hat{\boldsymbol{\Sigma}}_{k,IO}^{(j)} \\ \hat{\boldsymbol{\Sigma}}_{k,OI}^{(j)} & \hat{\boldsymbol{\Sigma}}_{k,OO}^{(j)} \end{bmatrix} \begin{bmatrix} \mathbf{A}_{t,I}^{(j)} & \mathbf{0} \\ \mathbf{0} & \hat{\mathbf{A}}_{t,O}^{(j)} \end{bmatrix}^T\end{aligned}\quad (10)$$

By rewriting both (9) and (10) in their expanded forms, we have that

$$\begin{aligned}\hat{\boldsymbol{\mu}}_{k,I}^{(j)} &= \boldsymbol{\mu}_{k,I}^{(j)} \\ \hat{\boldsymbol{\mu}}_{k,O}^{(j)} &= \left(\mathbf{A}_{t,O}^{(j)}\right)^{-1} \hat{\mathbf{A}}_{t,O}^{(j)} \boldsymbol{\mu}_{k,O}^{(j)} + \left(\mathbf{A}_{t,O}^{(j)}\right)^{-1} \left(\hat{\mathbf{b}}_{t,O}^{(j)} - \mathbf{b}_{t,O}^{(j)}\right) \\ \hat{\boldsymbol{\Sigma}}_{k,II}^{(j)} &= \boldsymbol{\Sigma}_{k,II}^{(j)} \\ \hat{\boldsymbol{\Sigma}}_{k,OI}^{(j)} &= \left(\mathbf{A}_{t,O}^{(j)}\right)^{-1} \hat{\mathbf{A}}_{t,O}^{(j)} \boldsymbol{\Sigma}_{k,OI}^{(j)} \\ \hat{\boldsymbol{\Sigma}}_{k,IO}^{(j)} &= \left(\hat{\boldsymbol{\Sigma}}_{k,OI}^{(j)}\right)^T \\ \hat{\boldsymbol{\Sigma}}_{k,OO}^{(j)} &= \left(\mathbf{A}_{t,O}^{(j)}\right)^{-1} \hat{\mathbf{A}}_{t,O}^{(j)} \boldsymbol{\Sigma}_{k,OO}^{(j)} \left(\left(\mathbf{A}_{t,O}^{(j)}\right)^{-1} \hat{\mathbf{A}}_{t,O}^{(j)}\right)^T\end{aligned}\quad (11)$$



**Algorithm 2** Forward search of task frames

---

```

1: Define  $P$  candidate task frames  $\{j\}_{j=1}^P$ 
2: Initialize an empty set  $\mathcal{F} = \emptyset$ 
3: repeat
4:   for  $j = 1$  to  $P$  do
5:     if  $\{j\} \in \mathcal{F}$  then
6:       continue
7:     end if
8:     evaluate the combined set  $\mathcal{F} \cup \{j\}$  using Algorithm 1
9:   end for
10:  Select the frame  $\{k\}$  with the smallest converged cost
11:   $\mathcal{F} \leftarrow \mathcal{F} \cup \{k\}$ 
12: until the number of frames in  $\mathcal{F}$  reaches the limit
13: return  $\mathcal{F}$ 

```

---

Thus, the optimization of task parameters (i.e., transform  $\{\mathbf{A}_{t,\mathcal{O}}^{(j)}, \mathbf{b}_{t,\mathcal{O}}^{(j)}\}$  into  $\{\hat{\mathbf{A}}_{t,\mathcal{O}}^{(j)}, \hat{\mathbf{b}}_{t,\mathcal{O}}^{(j)}\}$ ) is equivalent to the optimization of GMM components (i.e., transform  $\{\boldsymbol{\mu}_k^{(j)}, \boldsymbol{\Sigma}_k^{(j)}\}$  into  $\{\hat{\boldsymbol{\mu}}_k^{(j)}, \hat{\boldsymbol{\Sigma}}_k^{(j)}\}$ ). Note that in (6) rotation angles and translational vectors are learned so as to optimize task parameters. In contrast to classic approaches where GMM parameters (i.e., means, covariances and mixture coefficients) are updated [6], learning task parameters renders a lower dimensional optimization, which may speed up the learning process. More importantly, the optimization of task parameters is independent from the model parameters, and thus local consistent features from demonstrations are still maintained, which is highly desirable for the imitation learning.

## 5 Forward Search of Task Frames

Within the task-parameterized learning framework, the number of task frames are usually fixed and pre-determined [4, 9, 12]. A natural question concerning the number of task frames arises: can we change the number of task frames? More specifically, how can we determine the number of task frames? For instance, in a robot task with many candidate frames, redundant or irrelevant frames might exist, thus it is reasonable to remove these less task-relevant frames so as to alleviate the undesired influences from them. Even though this problem may have a significant impact on the robot performance, it has not been addressed in the previous works.

In analogy to the classical *forward search* used for selecting high dimensional features, we propose an iterative learning scheme to select the most-relevant task frames with respect to additional task constraints (which can be formulated as a cost function). We first consider the trajectory generation using a single frame. Through separate optimization of task parameters of each candidate frame via *Algorithm 1*, we can evaluate the influence of each frame based on their corresponding cost values. Note that the important frames influence the task significantly, and thus their

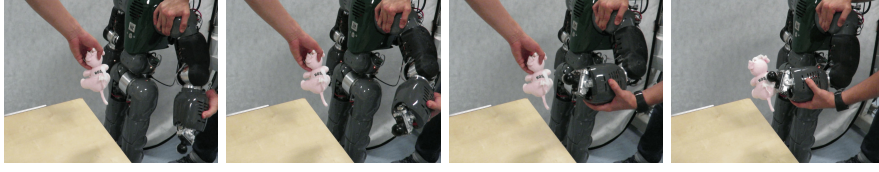


**Fig. 2** Kinesthetic teaching of a reaching skill on the COMAN robot.

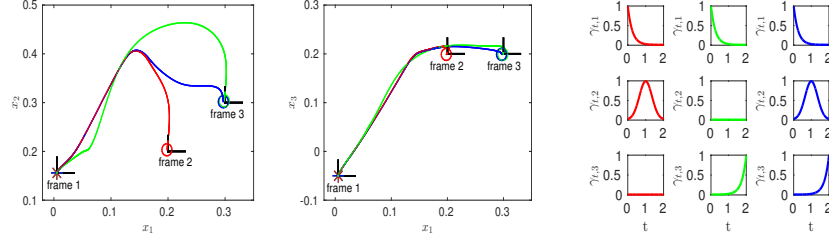


**Fig. 3** Trajectories (*left* and *middle* plots) generated by assigning different confidences (*right* graph) to task frames. The first, second and third columns of the *right* graph are associated with trajectories depicted by red, green and blue curves in the *left* and *middle* graphs, respectively. The start and end point of each trajectory are denoted by ‘\*’ and ‘o’, respectively.

corresponding cost values should decrease rapidly over the learning iterations, i.e., the lower the cost, the higher the importance of the frame. With this insight, we can find the best frame in terms of cost values. Subsequently, we consider the trajectory generation using two frames, i.e., the best frame and one of other frames. By evaluating the combination of the best frame and each of other frames, the optimal two-frame set can be determined. Similarly, we can find the optimal frame set with more frames until the number of task frames reaches the upper limit. Note that the frame selection scheme depends on the definition of the cost function, which is closely related to the task requirements and additional constraints. An entire algorithm for frame selection is summarized in *Algorithm 2*.

## 6 Evaluations

In this section, we evaluate our proposed methods using several examples: (i) we consider CW-TMP with different sets of frame confidences (Section 6.1); (ii) we apply the task frame optimization to a reaching task (Section 6.2.1) and an obstacle avoidance task (Section 6.2.2); (iii) we implement a transportation task to show the frame selection procedure (Section 6.3). CW-TMP and frame selection are evaluated on the simulated COMAN robot [16], the reaching task is carried out on both the simulated and real COMAN robot, and the obstacle avoidance task is performed only on the real COMAN robot. Since the tasks are all learned in the robot task space, we use the Jacobian matrix  $\mathbf{J}$  of the robot end-effector to control the joint

movement through joint position commands, i.e.,  $\hat{\mathbf{q}}_{t+1} = \mathbf{q}_t + \mathbf{J}(\mathbf{q}_t)^\dagger(\hat{\mathbf{p}}_{t+1} - \mathbf{p}_t)$  with  $\mathbf{J}^\dagger = \mathbf{J}^T(\mathbf{J}\mathbf{J}^T)^{-1}$ , where  $\mathbf{q}_t$  and  $\mathbf{p}_t$  respectively represent the joint and Cartesian positions at time  $t$ ,  $\hat{\mathbf{q}}_{t+1}$  and  $\hat{\mathbf{p}}_{t+1}$  represent the desired positions at time  $t + 1$ .

## 6.1 Evaluations on CW-TMP

We collected 10 reaching trajectories with data-points represented by  $\xi_t = [t \ \mathbf{p}^T]^T$  in the robot base frame  $\{O\}$  using kinesthetic teaching on the COMAN's left arm (as shown in Fig. 2), which last around 2s each. Assuming that the object orientation does not influence the reaching task, we define two initial frames located respectively at the start and end points of each demonstration. Through projecting demonstrations into these frames separately, we train a 4-state GMM to extract local consistency among projected trajectories in each frame, which is after used to retrieve local trajectories by GMR. Then, we consider the generalization of local trajectories to new task frames. Note that the robot arm starts from the same position, we therefore use the same start frame, i.e., frame  $\{1\}$  in Fig. 3 (*left* and *middle* graphs), described by task parameters  $\mathbf{A}^{(1)} = \mathbf{I}_{4 \times 4}$  and  $\mathbf{b}^{(1)} = [0 \ 0.005 \ 0.156 \ -0.050]^T$ . In order to illustrate the impact of frame confidences, we consider two new targets which are respectively located at  $[0.2 \ 0.2 \ 0.2]^T$  and  $[0.3 \ 0.3 \ 0.2]^T$ , and thus we define two corresponding target frames  $\{2\}$  and  $\{3\}$  represented by task parameters  $\mathbf{A}^{(2)} = \mathbf{A}^{(3)} = \mathbf{I}_{4 \times 4}$ ,  $\mathbf{b}^{(2)} = [0 \ 0.2 \ 0.2 \ 0.2]^T$ ,  $\mathbf{b}^{(3)} = [0 \ 0.3 \ 0.3 \ 0.2]^T$ . Three different groups of frame confidences are evaluated, where each group corresponds to a column in Fig. 3 (*right* graph). The final trajectories in  $\{O\}$  are computed using (5) and illustrated in the Fig. 3 (*left* and *middle* graphs). It is observed that the blue curve coincides with the red one at the beginning and gradually moves towards the green one, implying that frame confidences determine the contributions of frames, i.e., the frame assigned with a large (small) confidence has a large (small) influence on the final trajectory.

## 6.2 Evaluations on Task Frame Optimization

Here we show the experiments corresponding to the optimization of task parameters (*Algorithm 1*), where the same demonstrations of the reaching task are used. The optimization is carried out under two different scenarios, i.e., additional joint space constraints (Section 6.2.1) and obstacle avoidance (Section 6.2.2).

### 6.2.1 Reaching Task with Additional Joint Space Constraints

For the reaching task, we consider an additional constraint in the joint space, which minimizes the weighted joint displacement [15], i.e.,

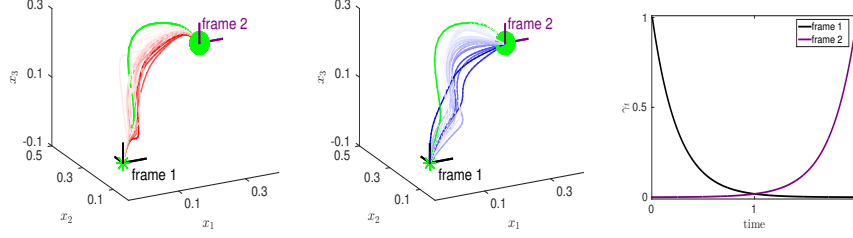


**Fig. 4** Frame confidences (*right* graph) assigned to two task frames, as well as robot reaching trajectories through optimizing GMM means (red curves in the *left* graph) and through optimizing task parameters (blue curves in the *middle* graph), where the color from light to dark shows the trajectory evolution direction, the green curves represent the reference trajectories without optimization. The start trajectory point and the target object are separately depicted by a green star and a green solid ball.

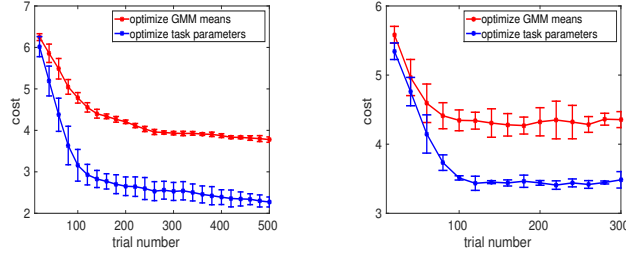


**Fig. 5** These graphs show cost values of optimizing GMM means and task parameters in different reaching tasks, where the *left* and *right* figures correspond to the target object located at  $[0.3 \ 0.3 \ 0.2]^T$  and  $[-0.3 \ 0.2 \ 0.2]^T$  in frame  $\{O\}$ , respectively. Error-bars represent means and standard deviations of cost values.

$$f_q = \sum_{t=1}^{N-1} ((\mathbf{q}_{t+1} - \mathbf{q}_t)^T \mathbf{W} (\mathbf{q}_{t+1} - \mathbf{q}_t))^{\frac{1}{2}}, \quad (12)$$

where  $\mathbf{W}$  represents a weighted matrix. Now, let us first consider the reaching of an object at  $[0.3 \ 0.3 \ 0.2]^T$  in frame  $\{O\}$ . We define two task frames described by  $\mathbf{A}^{(1)} = \mathbf{A}^{(2)} = \mathbf{I}_{4 \times 4}$ ,  $\mathbf{b}^{(1)} = [0 \ 0.005 \ 0.156 \ -0.050]^T$ ,  $\mathbf{b}^{(2)} = [0 \ 0.3 \ 0.3 \ 0.2]^T$ , as well as frame confidences shown in Fig. 4 (*right* graph). Note that both frames have their origins at the start and target points respectively, thus only the rotation operations are implemented. We use  $\text{PI}^2$  to learn rotation angles for both frames simultaneously, where the policy parameters in (8) are updated every 10 roll-outs. For comparison purposes, we evaluate the optimization of GMM components using  $\text{PI}^2$  as well. Here, similar to [6], we optimize Gaussian means while the higher dimensional covariance matrices are kept fixed. The trajectory convolutions in one run using each optimization is depicted in Fig. 4 (*left* and *middle* graphs). Besides this current target, we evaluate both optimizations again using a different target located

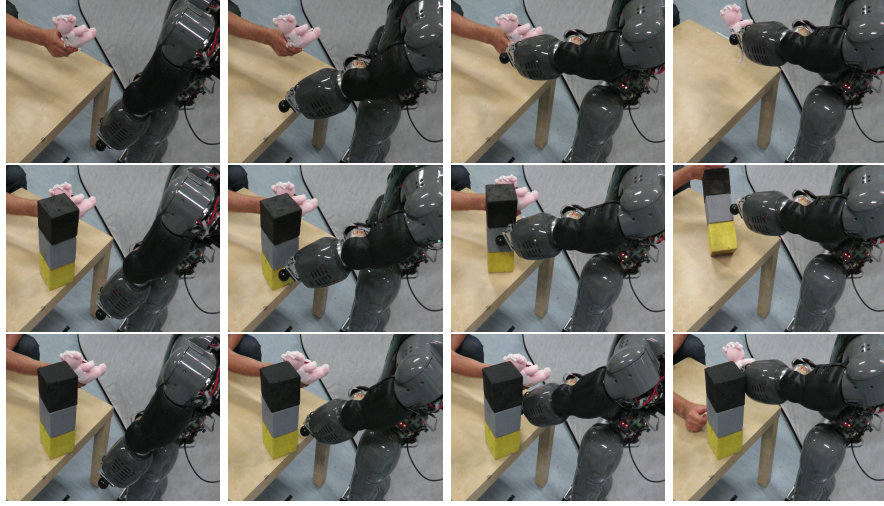


**Fig. 6** *Top*: reaching task learned by optimizing task parameters with respect to the cost function (12). *Middle*: reaching task with obstacle collision, where only the joint constraint (12) is used. *Bottom*: reaching task learned by optimizing task parameters with respect to the cost function (13).

at  $[-0.3 \ 0.2 \ 0.2]^T$  in  $\{O\}$ . We have 5 runs for each method and for each target. Meanwhile, we calculate the average cost every 20 roll-outs in each run. Finally, the means and standard deviations of average costs can be determined, as shown by the error-bar curves in Fig. 5. It is observed that our approach converges faster than GMM components optimization. This result coincides with our intuitions since the frame optimization has fewer parameters compared with the GMM optimization. In addition to these evaluations, we test the reaching task on the real COMAN robot, as depicted in Fig 6 (*top* row), showing that the proposed algorithm generates a trajectory that allows COMAN to perform successfully (A video of this experiment is added as supplementary material).

## 6.2.2 Obstacle Avoidance

We here consider the case in which an obstacle occupies a portion of the learned robot movement path (shown in Fig 6). In order to formulate the cost function easily, we simplify the obstacle as a bounded rectangle  $S$  and the robot end-effector as a point. Subsequently, we estimate the intersection point  $\tilde{\mathbf{p}}$  of the end-effector trajectory and  $S$ , and determine if the intersection point lies inside or outside  $S$ . Furthermore, let us denote the distance between  $\tilde{\mathbf{p}}$  and each edge of  $S$  as  $d_i, i \in \{1, 2, 3, 4\}$ , then the cost function can be defined as

$$C = \begin{cases} \sum_{t=1}^{N-1} ((\mathbf{q}_{t+1} - \mathbf{q}_t)^T \mathbf{W} (\mathbf{q}_{t+1} - \mathbf{q}_t))^{\frac{1}{2}} + k_1 e^{(k_2 d)}, & \tilde{\mathbf{p}} \in S \\ \sum_{t=1}^{N-1} ((\mathbf{q}_{t+1} - \mathbf{q}_t)^T \mathbf{W} (\mathbf{q}_{t+1} - \mathbf{q}_t))^{\frac{1}{2}} + k_3 e^{(-k_4 d)}, & \tilde{\mathbf{p}} \notin S \end{cases}, \quad (13)$$

where  $d = \min\{d_1, d_2, d_3, d_4\}$ ,  $k_i > 0, i \in \{1, 2, 3, 4\}$ . Here, the joint constraint is used to avoid large trajectory deviation from the original trajectory. As a comparison, we test the reaching task (i.e., the robot trajectory is optimized with the cost function (12)) with the obstacle as well. The evaluations on the real robot are illustrated in Fig. 6 (*middle* and *bottom* rows), where we can see that, the robot is capable of both avoiding the obstacle and reaching the target object by optimizing task parameters with respect to (13).

### 6.3 Evaluations on Automatic Frame Selection

We have evaluated a fixed set of task frames in the experiments previously reported, now we consider a pick-and-place task to show the application of the proposed frame selection scheme (*Algorithm 2*) given a large set of candidate frames. We collected 8 demonstrations of the task through kinesthetic teaching, which guided the robot to reach and pick up an object, and subsequently release it at the goal position, lasting about 10s each. We defined 5 initial candidate frames associated with the end-effector positions at time steps 2s, 4s, 7s, 9.5s and 10s, respectively. Then, we projected the demonstrations into these candidate frames, and subsequently trained local GMMs and generated local trajectories.

Considering a new task instance, which requires the robot to pick up the object located at  $\mathbf{p}_s = [0 \ 0.3 \ 0.1]^T$  (in frame  $\{O\}$ ) when  $t = 4s$ , and subsequently release it at  $\mathbf{p}_e = [0.3 \ 0.2 \ 0.2]^T$  (in frame  $\{O\}$ ) when  $t = 10s$ . Meanwhile, we expect to reduce the joint displacement. Through combining the task and joint constraints, the cost function is defined as

$$C = f_q + k_{p1}|\mathbf{p}_{t=4} - \mathbf{p}_s| + k_{p2}|\mathbf{p}_{t=10} - \mathbf{p}_e|, \quad (14)$$

where  $|\cdot|$  represents Euclidean distance,  $k_{p1}$  and  $k_{p2}$  are positive scalars. For this new task, we adapt 5 candidate frames using new task parameters  $\mathbf{A}^{(j)} = \mathbf{I}_{4 \times 4}$ ,  $j = \{1, 2, \dots, 5\}$ ,  $\mathbf{b}^{(1)} = [0 \ -0.05 \ 0.25 \ 0.05]^T$ ,  $\mathbf{b}^{(2)} = [0 \ 0.0 \ 0.3 \ 0.1]^T$ ,  $\mathbf{b}^{(3)} = [0 \ 0.10 \ 0.25 \ 0.15]^T$ ,  $\mathbf{b}^{(4)} = [0 \ 0.25 \ 0.22 \ 0.15]^T$  and  $\mathbf{b}^{(5)} = [0 \ 0.3 \ 0.2 \ 0.2]^T$ . Since these candidate frames only differ in their origins, it is not desired to apply a translational operation, and hence we study the rotation operation for this case. Following the *Algorithm 2*, we first evaluate each frame separately. The evaluation results are shown in Fig. 7 (*left* plot). Since the frame  $\{2\}$  has the most significant influence on the pick-and-place task (i.e., the smallest cost values and the fastest convergence speed), it is viewed as the most important frame. Furthermore, we evaluate the combination of frame  $\{2\}$  and the rest of frames. An illustration of trajectory evolutions in one run through combined optimization of frame  $\{2\}$  and  $\{3\}$  is reported in Fig. 8. The evaluations of two frames are shown in Fig. 7 (*right* graph), showing that the combined performance of frame  $\{2\}$  and frame  $\{5\}$  attains the lowest cost values. In summary, the optimal frame set can be roughly interpreted as a function of task parameters and additional constraints, the frame forward search in *Algorithm*

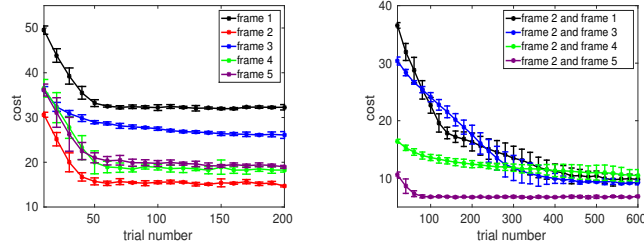


**Fig. 7** These figures depict cost values in the frame selection. The *left* plot shows cost values through optimizing a single task frame while the *right* plot shows cost values of optimizing the best frame {2} and each of the rest frames. Error-bars represents means and standard deviations of cost values.

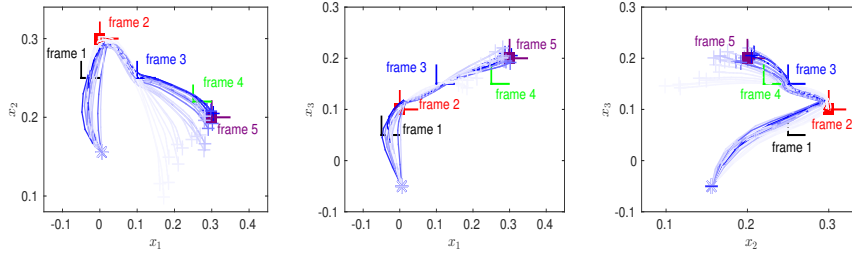


**Fig. 8** These figures show the trajectory evolutions (color: from light to dark) through optimizing task parameters of frame {2} and frame {3} simultaneously. The start and end point of each trajectory are depicted by the blue '\*' and '+', respectively. The solid red and purple solid boxes denote the desired via-point and end-point.

2 provides an optimal solution to this problem in the sense of finding a frame set achieving smallest cost values.

## 7 Conclusions

This paper has presented a generalized task-parameterized learning framework, which is initially learned from human demonstrations. The generalization first considers the confidence-weighted TMP, which allows for the incorporation of human prior knowledge on the task frames into TMP. Subsequently, a novel learning perspective is proposed, which directly optimizes task parameters instead of GMM components, rendering a lower dimensional optimization problem. Also, a dual interpretation is provided to show the connection between task parameters optimization and GMM components optimization. Moreover, an iterative feature selection scheme is proposed, which has shown effective to select important task frames and remove frames that are either redundant or irrelevant for the task. In our evaluations, we learn task parameters of different frames without considering their correlations.

Whereas, in many tasks (e.g., the robot bimanual task) the task frames are often relevant to each other, and thus the correlations between frames could be exploited, which might help to accelerate the learning process. Besides, the learning of task parameters has potentials in a set of task-parameterized regressions such as TP-LWR and TP-GPR [4].

## References

1. Argall, B. D., Chernova, S., Veloso, M., et al: A Survey of Robot Learning From Demonstration, *Robotics and autonomous systems*, **57**(5), 469-483 (2009)
2. Atkeson, C.G., Moore, A.W., Schaal, S.: Locally Weighted Learning. *Artificial Intelligence Review*, **11**, 11-73 (1997)
3. Buchli, J., Stulp, F., Theodorou, E., et al: Learning Variable Impedance control. *The International Journal of Robotics Research*, **30**(7), 820-833 (2011)
4. Calinon, S.: A Tutorial on Task-Parameterized Movement Learning and Retrieval. *Intelligent Service Robotics*, **9**(1), 1-29 (2016)
5. Cohn, D.A., Ghahramani, Z., Jordan, M.I.: Active Learning with Statistical Models. *Journal of Artificial Intelligence Research*, **4**(1), 129-145 (1996)
6. Guenter, F., Hersch, M., Calinon, S., et al: Reinforcement Learning for Imitating Constrained Reaching Movements. *Advanced Robotics*, **21**(13): 1521-1544 (2007)
7. Ijspeert, A.J., Nakanishi, J., Hoffmann, H., et al: Dynamical Movement Primitives: Learning Attractor Models for Motor Behaviors. *Neural Computation*, **25**(2), 328-373 (2013)
8. Muhlig, M., Gienger, M., Hellbach, S., et al: Task-level imitation learning using variance-based movement optimization. In: *IEEE International Conference on Robotics and Automation*, pp. 1177-1184 (2009)
9. Rozo, L., Calinon, S., Caldwell, D.G., et al: Learning Physical Collaborative Robot Behaviors from Human Demonstrations. *IEEE Transactions on Robotics*, **32**(3), 513-527 (2016)
10. Paraschos, A., Daniel, C., Peters, J., et al: Probabilistic Movement Primitives. In: *Proceedings of Advances in neural information processing systems*, pp. 2616-2624 (2013)
11. Rasmussen, C.E., Williams, C.K.I.: *Gaussian Processes for Machine Learning*. The MIT Press (2006)
12. Silvério, J., Rozo, L., Calinon, S., et al: Learning Bimanual End-Effector Poses from Demonstrations Using Task-Parameterized Dynamical Systems. In: *IEEE/RSJ International Conference on Intelligent Robots and Systems*, pp. 464-470 (2015)
13. Stulp, F., Sigaud, O.: Robot Skill Learning: From Reinforcement Learning to Evolution Strategies. *Journal of Behavioral Robotics*, **4**(1), 49-61 (2013)
14. Theodorou, E., Buchli, J., Schaal, S.: A Generalized Path Integral Control Approach to Reinforcement Learning. *Journal of Machine Learning Research*, **11**, 3137-3181 (2010)
15. Toussaint, M., Gienger, M., Goerick, C.: Optimization of Sequential Attractor-based Movement for Compact Behaviour Generation. In: *IEEE-RAS International Conference on Humanoid Robots*, pp. 122-129 (2007)
16. Tsagarakis, N.G., Morfey, S., Cerda, G.M., et al: Compliant Humanoid Coman: Optimal Joint Stiffness Tuning for Modal Frequency Control. In: *IEEE International Conference on Robotics and Automation*, pp. 673-678 (2013)